

Modulation analysis of large-scale discrete vortices

Luis A. Cisneros,^{1,*} Antonmaria A. Minzoni,^{2,†} Panayotis Panayotaros,^{2,‡} and Noel F. Smyth^{3,§}

¹*Department of Mathematics and Statistics, University of New Mexico, Albuquerque, New Mexico 87131-0001, USA*

²*Fenomenos Nonlineales y Mecánica (FENOMECA), Department of Mathematics and Mechanics, Instituto de Investigación en Matemáticas Aplicadas y Sistemas, Universidad Nacional Autónoma de México, 01000 México Distrito Federal, Mexico*

³*School of Mathematics and Maxwell Institute for Mathematical Sciences, The King's Buildings, University of Edinburgh, Edinburgh EH9 3JZ, United Kingdom*

(Received 13 May 2008)

The behavior of large-scale vortices governed by the discrete nonlinear Schrödinger equation is studied. Using a discrete version of modulation theory, it is shown how vortices are trapped and stabilized by the self-consistent Peierls-Nabarro potential that they generate in the lattice. Large-scale circular and polygonal vortices are studied away from the anticontinuum limit, which is the limit considered in previous studies. In addition numerical studies are performed on large-scale, straight structures, and it is found that they are stabilized by a nonconstant mean level produced by standing waves generated at the ends of the structure. Finally, numerical evidence is produced for long-lived, localized, quasiperiodic structures.

DOI: XXXX

PACS number(s): 05.45.Yv, 42.65.Tg

I. INTRODUCTION

The discrete nonlinear Schrödinger (DNLS) equation is a nonlinear lattice model that appears in many areas of science and which has attracted a lot of attention in recent years. One such area is nonlinear optics, where the usefulness of the DNLS equation as a model for coherent light propagation in waveguide arrays has been well established [1–4]. The DNLS equation has also been used to describe Bose-Einstein condensates in optical lattices [5], as well as energy transfer in biomolecular chains [6,7].

A major effect of a nonlinear lattice is the localization of energy in a few “active” sites. This was first noted by Sievers and Takeno [8]. Subsequent theoretical studies have explained localization by showing the existence of breather solutions, defined as spatially decaying time-periodic solutions for which each site has the same temporal frequency [9–12]. The existence of these stable (and unstable) breathers in one- and higher-spatial-dimensional lattices is well understood. In the case of breathers near the limit of vanishing site coupling, the “anticontinuum limit” [9], the set of active sites can be an arbitrary finite subset of the integer lattice. Breathers are also robust in that they appear in several variants of the DNLS equation [13,15,14] and in other lattice models. Breathers with two quasiperiods in time have also been shown to exist [16].

In the present work we examine localized structures from a different perspective, with emphasis on the spatial features of the localized structure and leaving the temporal behavior undetermined *a priori*. This allows us to understand theoretically the dynamical behavior of localized structures that are difficult to analyze using the breather ansatz. Moreover, we allow structures that have a more general temporal behavior.

The first these solutions examined are the vortexlike solutions, which are discrete analogs of the circular vortex solutions of the continuous NLS equation. In the limit of large radius and small width to radius ratio, an asymptotic theory based on a modulated vortex ansatz in an averaged Lagrangian predicts the existence of stable and unstable localized solutions with suitable width to radius ratios. These structures are also found numerically and their stability properties coincide with the theoretical predictions. Spatiotemporal modulation of these structures corresponds to wavelike modes which propagate in the angular direction around the vortex, with the vortex eventually evolving to a time-periodic localized state. We find furthermore that the discretization effects arising through the Peierls-Nabarro potential can stabilize perturbations which correspond to unstable modes of the continuous NLS vortex. In the wavelike structures we find sizable spatial and temporal variations in the amplitude and phase of the sites, which suggests that we are far from the small-coupling discrete vortex breathers of the type described by Pelinovsky *et al.* [12].

The second type of solution we examine is localized in thin parallelogram sets. We assume that the width to length ratio of the parallelogram is small and use an averaged Lagrangian with a suitable ansatz to find periodic, spatially localized solutions. We find again basic stable states and wavelike structures that move along the length of the parallelogram, bouncing from the two ends. In this parallelogram case, however, the modulation does not decay, suggesting either much slower radiation of these modes, or a new stable state with a standing wave that cannot be captured by the breather ansatz.

Additionally we study numerically localization along polygons whose sides are thin parallelograms. The behavior is qualitatively similar to that seen in the circular vortex case, in that we see stable localization with some modulation. In another set of numerical experiments we examine localization on smaller sets, analyzing the evolution of each site in more detail. We see sites that evolve in an approximately periodic manner, but with periods that are not the same for all sites. These localized states do not show any tendency to

*cisneros@math.unm.edu

†tim@mym.iimas.unam.mx

‡panos@mym.iimas.unam.mx

§N.Smyth@ed.ac.uk

90 decay and may constitute another type of stable or meta-
 91 stable localized state which is not a breather. Further com-
 92 ments on possible interpretations of the numerical results are
 93 given in the Conclusions.

94 II. FORMULATION AND CIRCULAR VORTICES

95 Let us consider the two-space-dimensional DNLS equa-
 96 tion on the infinite square lattice, labeled by the integers n, m
 97 with $-\infty < m, n < \infty$, in the form

$$98 \quad i\dot{u}_{mn} = \Delta_{mn}u_{mn} + \delta^{-1}|u_{mn}|^2u_{mn}. \quad (1)$$

99 Here Δ_{mn} is the second-order difference operator in the vari-
 100 ables m and n and time derivatives are denoted by an over-
 101 dot.

102 In the present work we are interested in finding localized
 103 solutions of the DNLS equation (1) with extended, nontrivial
 104 shapes, and periodic, and possibly more general, time depen-
 105 dence. It is well known that in the continuum limit $\delta \rightarrow \infty$ all
 106 pulselike solutions collapse (blow up) and that other local-
 107 ized initial conditions behave in a similar manner. This col-
 108 lapse behavior is due to the focusing nonlinearity. On the
 109 other hand, in the so-called anticontinuum limit $\delta \rightarrow 0$ the
 110 discrete NLS equation (1) has time-periodic solutions of the
 111 form

$$112 \quad u_{mn} = A_{mn}e^{-i\sigma t}e^{i\theta_{mn}}, \quad (2)$$

113 where, for an arbitrary set of sites m, n , $A_{mn} = A$, $\sigma = A^2/\delta$,
 114 and θ_{mn} is arbitrary, while $u_{mn} = 0$ for the remaining sites.
 115 These solutions are clearly localized around an arbitrary
 116 shape. Using bifurcation theory ideas, it was shown by Peli-
 117 novsky *et al.* [12] that for small δ these solutions can be
 118 continued uniquely (up to a global phase) in δ , provided that
 119 the θ_{mn} are chosen appropriately. One then obtains a branch
 120 of periodic solutions for which A_{mn} and θ_{mn} depend on δ .
 121 This procedure can be used to effectively calculate branches
 122 of solutions in cases for which the set of active sites is small
 123 or has a simple geometry. For example, in the case of a close
 124 polygonal line shape where each active site has only two
 125 active neighbors, solutions can be found for which θ_{mn} in-
 126 creases by an arbitrary integer multiple 2π around a circuit
 127 [12]. These “discrete vortices” are examples of breathers [9],
 128 since breathers are, by definition, time-periodic solutions for
 129 which each site has the same frequency.

130 Let us now study the behavior of vortex-type solutions
 131 that are localized on larger sets and exist for larger δ . We
 132 shall also leave the time dependence undetermined and so
 133 consider possible solutions that are generalizations of breath-
 134 ers. In order to look at larger vortex-type solutions, we need
 135 to capture with a continuum coherent solution both the fact
 136 that there is a large number of active sites, and by the
 137 Peierls-Nabarro potential the effect of the discrete lattice on
 138 this coherent solution. This is achieved using Whitham
 139 modulation theory [17] on the averaged Lagrangian for the
 140 discrete NLS equation (1),

$$L = \int \sum_{mn} [i(u_{mn}^* \dot{u}_{mn} - u_{mn} \dot{u}_{mn}^*) + \nabla_{mn} u_{mn} \nabla_{mn} u_{mn}^* - \delta^{-1}|u_{mn}|^4] dt. \quad (3)$$

Here the superscript asterisk denotes the complex conjugate
 and ∇_{mn} is the discrete gradient vector based on forward
 differences. Appropriate trial functions with time-dependent
 parameters will be used to represent localized periodic solu-
 tions and their evolution (modulations).

Let us begin by studying circular vortices and their stabil-
 ity. The appropriate trial function for this case is

$$u_{mn} = a\sqrt{m^2 + n^2}(\operatorname{sech} \psi)e^{i\varphi} + ig e^{i\theta_{mn} + i\sigma t}, \quad (4)$$

$$\varphi = \theta_{mn} + [\sqrt{m^2 + n^2} - R(t)]V(t) + \sigma(t), \quad (5)$$

$$\psi = \frac{\sqrt{m^2 + n^2} - R(t)}{w}, \quad (6)$$

$$\theta_{mn} = \tan^{-1}n/m. \quad (7)$$

This trial function represents a vortex of width w concen-
 trated on a circle of radius R , with the phase increasing by
 2π around it. The vortex parameters a and w and the shelf
 height g are assumed to be functions of time t and the polar
 angle θ . As in previous studies of the stability of nonlocal
 continuum vortices, it will be assumed that the amplitude a is
 related, to leading order, to the width w by conservation of
 mass for the vortex [18]. This assumption is equivalent to a
 linear stability analysis for the vortex. The shelf, of height g ,
 will be assumed to be concentrated at the peak of the vortex
 and to have a width Λ_1 which will be determined as part of
 the analysis [18]. Hence g is nonzero only in the region
 $r_{\min} < r < r_{\max}$, where $r_{\min, \max} = R \mp \Lambda_1/2$. The phase variable
 of the vortex ring accounts for its contraction or expansion.

The averaged Lagrangian is determined by substituting
 the trial function into the Lagrangian. The double sums in-
 volved are calculated using Poisson’s formula, which gives

$$\sum_{mn} f(m, n) = \sum_{mn} \hat{f}(2\pi m, 2\pi n), \quad (8)$$

where \hat{f} denotes the Fourier transform of f , given by

$$\hat{f}(\xi, \eta) = \int_{-\infty}^{\infty} \int_{-\infty}^{\infty} f(x, y) e^{-i(\xi x + \eta y)} dx dy. \quad (9)$$

The first term of the series (8) with $m=n=0$ gives the con-
 tinuum approximation. The rest of the series gives the self-
 consistent Peierls-Nabarro potential generated by the interac-
 tion between the continuum vortex and the lattice. As in
 other discrete problems [19], to leading order finite differ-
 ences of u_{mn} are replaced by the equivalent derivatives. Fi-
 nally, the dominant contributions for the Poisson sum (8) are
 given by the terms $m = \pm 1, n = 0$ and $m = 0, n = \pm 1$. More-
 over, for small δ , to leading order, only the δ^{-1} term contrib-
 utes to the averaged Lagrangian terms which arise from the
 sum. In this manner, on using polar coordinates to calculate

185 the continuum contribution, the averaged Lagrangian (3) be-
186 comes

$$187 \quad L = \int_{t_0}^{t_1} \int_0^{2\pi} \int_0^\infty \left(ir(u^* u_t - uu_t^*) \right. \\ 188 \quad \left. + r|u_r|^2 + \frac{1}{r}|u_\theta|^2 - \frac{r}{\delta}|u|^4 \right) dr d\theta dt \\ 189 \quad - \int_{t_0}^{t_1} \sum_{|n|=|m|=1}^\infty \delta^{-1} \widehat{|u|^4} (2\pi m, 2\pi n) dt = L_0 + L_p. \quad (10)$$

190 In the integral term of this averaged Lagrangian the trial
191 function (4) is replaced by the continuous function obtained
192 by replacing $\sqrt{m^2+n^2}$ by r and θ_{mn} by the polar angle θ .
193 Since we are assuming that $w \sim \delta \ll 1$, the integrals involved
194 in the averaged Lagrangian (10) are easily calculated. In fact,
195 since $R \gg w$ and the vortex is peaked at $r=R$, the integrals
196 can be reduced to integrals involving sech and its powers and
197 derivatives. Moreover, it is assumed that the shelf has the
198 form $rg(\theta)$. It can then be found that the density \mathcal{L}_0 of the
199 averaged Lagrangian is

$$200 \quad \frac{\mathcal{L}_0}{2\pi} = - (2a^2 w R^3 + 4\Lambda_1 R^3 g^2) \dot{\sigma} - 2awR^2 g \dot{w} \\ 201 \quad - 2a^2 R^3 w \left(V\dot{R} - \frac{1}{2} V^2 \right) - I \frac{a^2 R}{w} w_\theta^2 - \frac{2\Lambda_1}{R} g_\theta^2 \\ 202 \quad + 4\delta^{-1} a^2 w R^5 g^2 - 4a^2 w R - \frac{2a^2 R^3}{3w} + \frac{2}{3} \delta^{-1} a^4 w R^5, \quad (11)$$

203 where

$$204 \quad I = \int_{-\infty}^\infty \eta^2 (\text{sech}^2 \eta) (\tanh^2 \eta) d\eta. \quad (12)$$

205 As in the continuum case [18], small contributions due to
206 terms involving a_θ have been neglected, as these terms are
207 $O(R^{-2})$ compared with the retained terms. The width R_s of
208 the shelf will be determined in the following section.

209 To calculate the density \mathcal{L}_p the Fourier transform of $|u|^4$ is
210 calculated in polar coordinates. Since R is assumed to be
211 large, the angular integral is calculated using the method of
212 stationary phase. The radial integral is then calculated to
213 leading order by closing the contour in the appropriate half
214 plane, resulting in

$$215 \quad \mathcal{L}_p = \frac{16\pi^{5/2}}{3\delta} a^4 w^4 R^{9/2} e^{-\pi^2 w} \cos(2\pi R - \pi/4) = H(R, w). \quad (13)$$

216 This term of the averaged Lagrangian gives the self-
217 consistent Peierls-Nabarro potential generated by the interac-
218 tion of the circular vortex and the lattice.

219 III. MODULATION EQUATIONS AND CIRCULAR 220 VORTICES

221 Taking variations of the averaged Lagrangian term (11)
222 with respect to σ gives the conservation of mass equation

$$\frac{d}{dt} a^2 w R^3 = 0. \quad (14) \quad 223$$

As in the continuum case [18], this mass conservation equa-
tion relates variations in the vortex amplitude and width. The
variational equations in V and R give equations for the mo-
tion of the vortex as

$$\dot{R} = V \quad (\delta V), \quad (15) \quad 228$$

$$\frac{d}{dt} (a^2 w R^3 V) + \frac{\partial \mathcal{L}_0}{\partial R} + \frac{\partial \mathcal{L}_p}{\partial R} = 0 \quad (\delta R). \quad (16) \quad 229$$

On assuming that the vortex parameters are independent of
the angular variable, we obtain the dispersion relation from
the variational equations

$$\dot{\sigma} + \frac{1}{3w^2} - \frac{2}{3} \delta^{-1} a^2 R^2 = 0 \quad (\delta a), \quad (17) \quad 233$$

$$\dot{\sigma} - \frac{1}{3w^2} - \frac{1}{3} \delta^{-1} a^2 R^2 = 0 \quad (\delta w). \quad (18) \quad 234$$

Here the Peierls-Nabarro contributions are of small order as
 $R \rightarrow \infty$.

The variational equations (15) and (16) have fixed points
which correspond to a static vortex with $V=0$ and the radius
 R given by the solution of

$$\frac{\partial \mathcal{L}_0}{\partial R} + \frac{\partial \mathcal{L}_p}{\partial R} = 0. \quad (19) \quad 240$$

The variational equation (19) has to be solved coupled to the
variational equations (17) and (18). The variational equations
(17) and (18) give the dispersion relation for the vortex

$$a = \sqrt{\frac{3}{2}} \frac{\delta^{1/2}}{wR} \quad \text{and} \quad \dot{\sigma} = -\frac{1}{w^2}. \quad (20) \quad 244$$

Using the variational equation (17) in the variational
equation (19) gives

$$0 = \frac{\partial \mathcal{L}_0}{\partial R} + \frac{\partial \mathcal{L}_p}{\partial R} = \frac{16}{3} \delta^{-1} a^4 w R^4 + \delta^{-1} a^4 w R^{7/2} \\ - \frac{32\pi^{7/2}}{3} \delta^{-1} a^4 w^4 R^{9/2} e^{-\pi^2 w} \sin(2\pi R - \pi/4). \quad (21) \quad 247 \quad 248$$

Let us assume that w is $O(\delta^{1/2})$, so that $w = (\alpha\delta)^{1/2}$. Then
using the results (20) in Eq. (21) gives the equation for the
radius R as

$$1 - 2\pi^{7/2} (\alpha\delta)^{1/2} R^{1/2} e^{-\pi^2 \sqrt{\alpha\delta}} \sin(2\pi R - \pi/4) = 0. \quad (22) \quad 252$$

For large R this equation has the solution

$$\sin(2\pi R - \pi/4) = 0, \quad (23) \quad 254$$

which results in

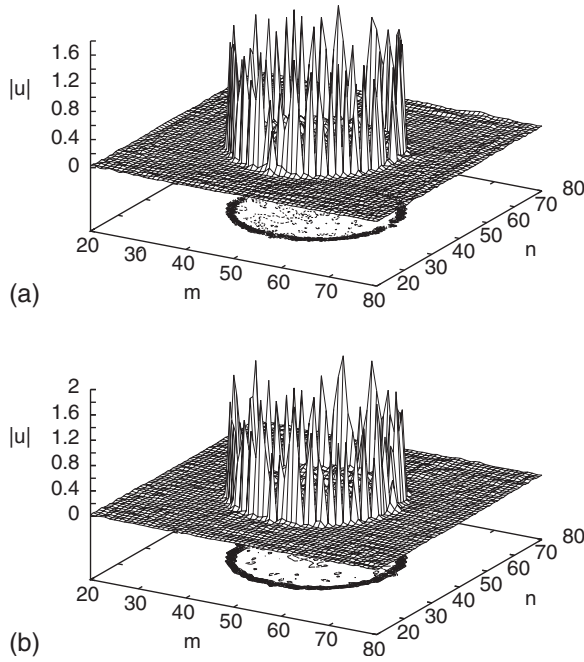


FIG. 1. Solution of DNLS equation (1) for vortex initial condition (4) with $a=0.1$, $w=0.3$, $V=0$, $R=15.5$, $g=0$, and $\delta=0.05$. (a) Solution at $t=30$; (b) perturbed solution with $a=0.1[1+0.2\cos(4\theta)]$ at $t=20$.

$$R = \frac{q\pi}{2} + \frac{1}{8} \quad (24)$$

256

at the fixed point, where q is a positive integer. The radii R_q are minima of the potential, provided that q is odd. For q even, the vortex will be unstable since it is located at a maximum of the Peierls-Nabarro potential. Hence the only stable vortices are for q odd.

For the parameter values of Fig. 1, Eq. (20) gives a vortex amplitude of $a=1.2$, which compares well with the average amplitude of the vortex in Fig. 1(a). However, it can be that the trial function does not include the circumferential oscillations seen in the numerical solution. Furthermore, from Eq. (22) it can be seen that as the DNLS equation becomes continuous in the limit of large δ the vortex becomes unstable. This is because for a given radius R , as δ increases, the stable and unstable roots of (22) coalesce, losing the vortex. For the parameter values of Fig. 1, Eq. (22) predicts that the vortex ceases to exist at $\delta=0.57$. Numerical results show that at $\delta=0.5$ the vortex structure begins to develop large gaps between the peaks and the vortex completely disappears at $\delta=0.689$. The modulation theory results are then in good quantitative agreement with the numerical results.

The solution (20) and (24) gives a family of vortices parametrized by their radius and their width. In the continuum limit these vortices will be unstable to azimuthal perturbations in w , with angular wave number $\ell=2$ being the fastest growing mode [18]. It will now be shown how discreteness, as captured by the Peierls-Nabarro potential in Eqs. (21) and (22), stabilizes the vortex.

To study the stability of the discrete vortex, we proceed as in Minzoni *et al.* [18] and expand the averaged Lagrangian

about the fixed point to quadratic order, taking $w=w_q+\tilde{w}$, which results in

$$\begin{aligned} \mathcal{L}_f = \int_{t_0}^{t_1} & \left(2awR^2\tilde{w}\dot{g} - \frac{IRa^2}{w}\tilde{w}_\theta^2 - \frac{2\Lambda_1}{R}g_\theta^2 - 4\Lambda_1R^3\dot{\sigma}g^2 \right. \\ & \left. + 4\delta^{-1}a^2wR^5g^2 - \frac{\tilde{w}^2}{2}H_{ww}(R_q, w_q) \right) dt. \end{aligned} \quad (25)$$

Here Λ_1 is a function of R which will be determined in the analysis. The Hamiltonian equations derived from the Lagrangian (25) will have oscillatory solutions, provided that the corresponding quadratic form is positive definite. Otherwise the linearized equations show that the discrete vortex is unstable. For $w=O(\delta)$ and R_q at a minimum of the Peierls-Nabarro potential, $H_{ww}(R_q, w_q) > 0$. In this case the corresponding quadratic form has to be studied in detail in order to determine the stability of the vortex.

The Euler-Lagrange equations for the linearized averaged Lagrangian (25) are

$$\dot{g} = -\frac{2IRa^2}{w}\tilde{w}_{\theta\theta} - H_{ww}\tilde{w}, \quad (30)$$

$$\dot{w} = \frac{2\Lambda_1}{R}g_{\theta\theta} - (2\Lambda_1R^3\dot{\sigma} - 4\delta^{-1}R^5a^2w)g, \quad (32)$$

where the time is rescaled with $2awR^2$. The solutions of these linearized modulation equations are readily obtained in terms of the normal modes,

$$\begin{pmatrix} g \\ w \end{pmatrix} = e^{\lambda t} e^{i\ell\theta} \begin{pmatrix} G \\ W \end{pmatrix}, \quad (27)$$

where G and W are constants. The equation for the eigenvalue λ is

$$\lambda^2 + \left(\frac{2Ia^2}{Rw}\ell^2 - H_{ww} \right) \left(\frac{2\Lambda_1}{R}\ell^2 - (4\delta^{-1}R^5a^2w - 2\Lambda_1R^3\dot{\sigma}) \right) = 0. \quad (28)$$

In this eigenvalue equation, one root $\lambda_2 < 0$ for small and large ℓ , but is positive when

$$\frac{Rw}{Ia^2}H_{ww} \leq \ell^2 \leq \frac{R}{2\Lambda_1}(4\mu\delta^{-1}R^5a^2w - 2\Lambda_1\dot{\sigma}). \quad (29)$$

To determine the stability of the vortex, the width of the shelf needs to be determined, so that Λ_1 can be calculated.

In an unstable region, if present, the vortex should have small but finite amplitude deformations. This possibility was explored by taking Λ_1 as a bifurcation parameter to produce the desired deformation waves. The solutions of the nonlinear equations arising from (26) on keeping higher-order terms do not have periodic solutions of period 2π . We therefore conclude that there is no instability region. To finish the stability analysis, we need to find Λ_1 which satisfies

$$4R^5a^2w - 2\Lambda_1\dot{\sigma} = \frac{Rw}{Ia^2}H_{ww}. \quad (30)$$

This gives $\Lambda_1 = w + wH_{ww}/(Ia^2R^{7/2})$. The mode

325
$$\ell^2 = \frac{Rw}{Ia^2} H_{ww} \quad (31)$$

326 then has zero growth rate, which implies marginal stability.
 327 This marginal mode is interpreted as an approximation to a
 328 very long-period perturbation. Substituting values for Λ_1 and
 329 $\hat{\sigma}$ gives $\ell=4$ as a long-lifetime mode. Using the numerical
 330 values in Fig. 1 the critical mode wave number is obtained
 331 from Eq. (31) as 4.382..., which is a good approximation to
 332 the actual value of 4. To test this conclusion the steady vor-
 333 tex was perturbed with an amplitude $a_p(\theta) = a(1 + \epsilon \cos 4\theta)$,
 334 which is a wave with $\ell=4$. The results are shown in Fig.
 335 1(b). On comparing this figure with Fig. 1(a) the effect of
 336 this long-lifetime mode can be seen, as the perturbation in
 337 amplitude has resulted in an increase in amplitude of the
 338 azimuthal wave around the vortex. Amplitude perturbations
 339 with modes either side of $\ell=4$ result in smaller-amplitude
 340 perturbations of the azimuthal wave.

341 **IV. THIN RECTANGULAR VORTICES**

342 It has been shown that the Peierls-Nabarro potential is
 343 responsible for the stability of a discrete vortex due to the
 344 trapping of the vortex maximum by the corresponding poten-
 345 tial. It is then expected that the same mechanism will be able
 346 to sustain stable structures of various shapes, when δ is suf-
 347 ficiently small.

348 As a first, simple example let us consider a periodic solu-
 349 tion concentrated along a straight line. The approximate trial
 350 function is

351
$$u_{mn} = \begin{cases} a(\operatorname{sech} \psi)e^{i\tau} + ig e^{i\sigma t} & \text{for } x_2(t) \leq m \leq x_1(t), \\ 0 & \text{otherwise,} \end{cases}$$

352
$$\psi = \frac{n - y(t)}{w},$$

353
$$\tau = \sigma t + \theta_{mn} + (m - x_1)V_x^{(1)} + (m - x_2)V_x^{(2)} + [n - y(t)]V_y. \quad (32)$$

354 We choose the phase θ_{mn} to obtain a phase τ which behaves
 355 as $(m - x_1)V_x^{(1)}$ for $x_1 < m \leq x_1 + \rho$, $(m - x_2)V_x^{(2)}$ for $x_2 - \rho \leq m$
 356 $\leq x_2$, and constant in the region $x_1 + \rho \leq m \leq x_2 - \rho$. In this
 357 approximation the end points move independently. The shelf
 358 g is concentrated about $y(t)$, which is the position of the
 359 maximum of the vortex. The end points x_1 and x_2 of the line
 360 segment are allowed to evolve as functions of time t . Nu-
 361 merical solutions show that the line vortex develops a modu-
 362 lated mean level due to an undular bore propagating in from
 363 the ends (see Fig. 2). To account for this the amplitude a is
 364 modified to become $a(1 + \mu(x/x_1)^2)$ to include the depression
 365 produced by the waves entering the vortex from its edges.
 366 For this special case of a symmetric trial function the aver-
 367 aged Lagrangian is

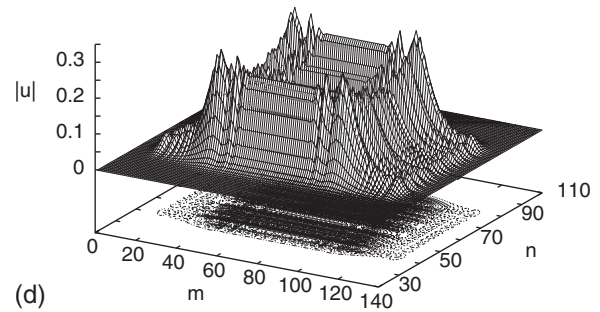
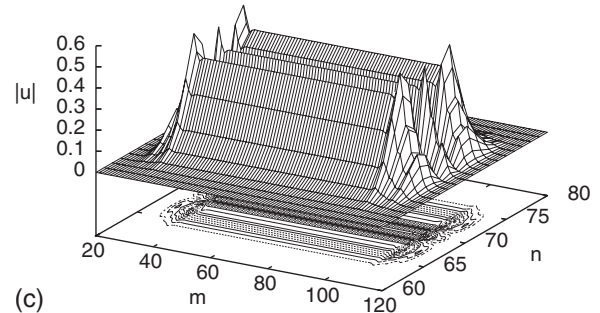
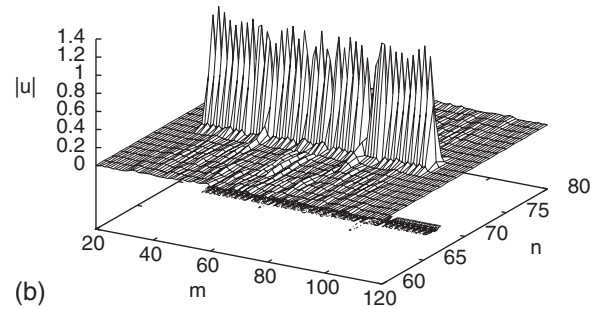
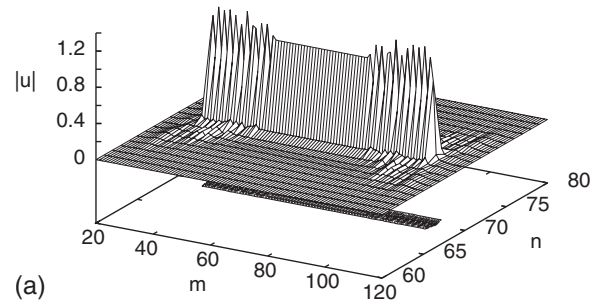


FIG. 2. Solution of DNLS equation (1) for wall initial condition (32) with $a=1.0$, $w=0.3$, $g=0$. Solution at (a) $t=3$ for $\delta=0.05$, (b) $t=30$ for $\delta=0.05$, (c) $t=2$ for $\delta=5$, and (d) $t=10$ for $\delta=5$.

AQ:
#2

368
$$\mathcal{L} = 2a^2wx_1 \left(\sigma + \rho x_1 V_x^{(1)} - \frac{1}{2} \rho V_x^{(1)2} + \zeta V_y - \frac{1}{2} V_y^2 \right)$$

 369
$$- \frac{4}{3} x_1 \left(\frac{a^2}{w} + 2\delta^{-1} a^4 w \right) - \frac{8}{3x_1} \mu^2 a^2 w. \quad (33)$$

The contribution of the Peierls-Nabarro potential takes the form

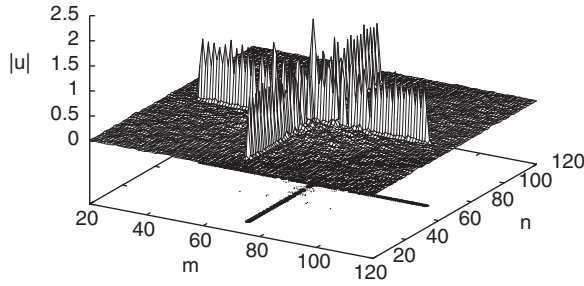


FIG. 3. Solution of DNLS equation (1) for cross initial condition at $t=30$.

$$\mathcal{L}_p = \frac{3}{\pi\delta} a^4 w \cos 2\pi x_1. \quad (34)$$

372

373 It is to be noted that unlike the Peierls-Nabarro contribution
374 for a circular vortex (13), the Peierls-Nabarro potential for
375 this line vortex is generated by the ends of the vortex. There-
376 fore as δ increases it is only algebraically small in δ since
377 $w \sim \delta^{1/2}$.

378 As before, for δ sufficiently small, the equations of motion
379 derived from this averaged Lagrangian show trapping of
380 the straight line segment by the Peierls-Nabarro potential.
381 The modulation equations for the steady-state line vortex are

$$\sigma + \frac{4}{3w^2} + \frac{8}{3\delta} a^2 - \frac{8}{3} \frac{\mu^2}{x_1^2} + 6\delta^{-1} a^2 w \sin 2\pi x_1 = 0, \quad \delta x_1, \quad (35)$$

382

$$\sigma - \frac{4}{3w^2} - \frac{8}{3\delta} a^2 - \frac{8}{3x_1^2} \mu^2 a = 0, \quad \delta w, \quad (35)$$

383

$$\sigma + \frac{4}{3w^2} - \frac{16}{3\delta} a^2 - \frac{8}{3x_1^2} \mu^2 a = 0, \quad \delta a. \quad (35)$$

384

385 Since we are interested in large vortices, we have to leading
386 order that

$$\sigma = -\frac{4}{3w^2} - \frac{8}{3\delta} a^2, \quad (36)$$

387

388 with a dispersion relation similar to that for the circular vor-
389 tex

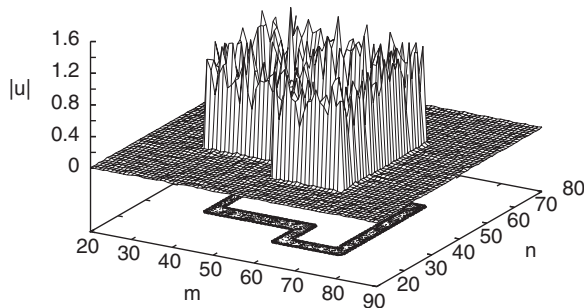


FIG. 4. Solution of DNLS equation (1) for the L-shaped initial condition at $t=30$.

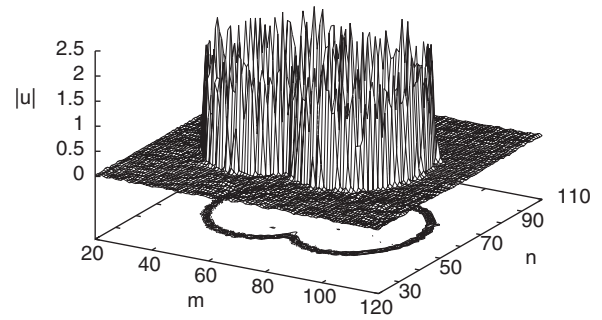


FIG. 5. Solution of DNLS equation (1) for figure of 8 initial condition at $t=30$.

$$\delta^{-1} a^2 w^2 = \frac{1}{4}. \quad (37)$$

390

The higher-order terms in the δx_1 equation in the modulation
equations (35) give the size of the vortex as the solution of

$$\frac{\mu^2}{x_1^2} = \frac{9}{2} \delta^{-1} a^2 w \sin 2\pi x_1. \quad (38)$$

393

This solution shows that as δ increases the solutions x_1 be-
come larger. A line vortex of a given size then destabilizes as
 δ increases due to the coalescence of a stable and an unstable
solution. This situation is analogous to that for the circular
vortex.

The modulation equations for the shelf g and the width
perturbation \tilde{w} can be developed in a similar manner as for
the circular vortex. However, these equations will not be
analyzed as the main stability result does not come from the
oscillations in the body of the vortex, but from the end
points. This stability mechanism is described above.

The initial evolution of the line vortex is shown in Fig.
2(a) in which the waves generated at the ends of the vortex
are seen to propagate into the vortex, in the manner of an
undular bore. In the modulation equations μ cannot be deter-
mined variationally as the form of a suitable, simple trial
function which captures the end point behavior is not clear.
As δ increases it follows from the modulation equation (38)

394

395

396

397

398

399

400

401

402

403

404

405

406

407

408

409

410

411

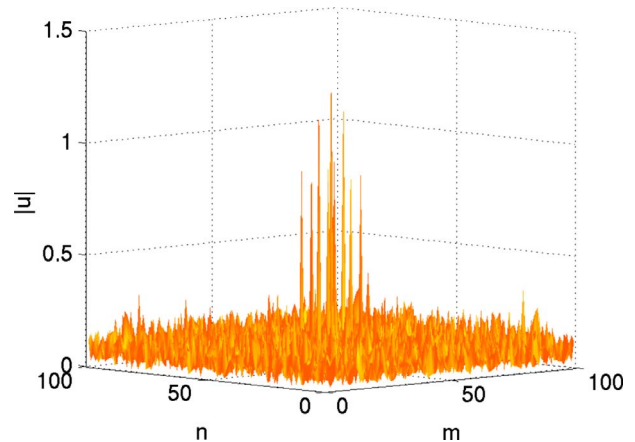


FIG. 6. (Color online) 12-peak solution of DNLS equation, $\delta=0.2$.

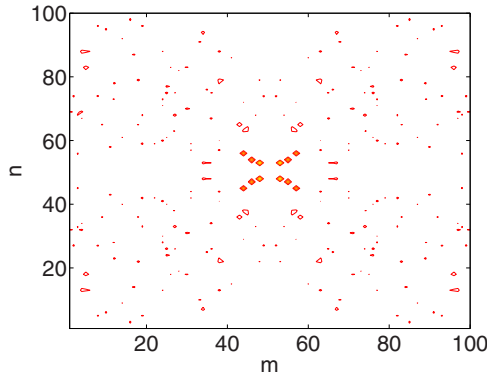


FIG. 7. (Color online) Contour plot of 12-peak solution of DNLS equation, $\delta=0.2$.

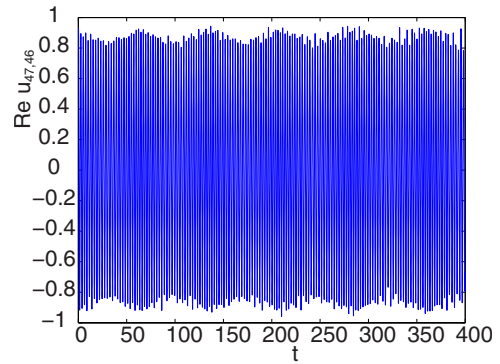


FIG. 9. (Color online) $\text{Re}(u_{47,46})$ at sites of middle square as a function of time.

412 that the Peierls-Nabarro potential can no longer hold the vor-
 413 tex, as can be seen in Fig. 2(c). It can also be seen that an
 414 undular bore develops at the leading and trailing edges of the
 415 vortex and expands into it. This bore expands the vortex,
 416 with it expanding symmetrically into $y > 0$ and $y < 0$, as re-
 417 quired by momentum conservation.

418 This same mechanism operates for more complicated
 419 structures, such as the cross shown in Fig. 3. Here the two
 420 arms of the cross act independently and can sustain a stable
 421 structure. This type of solution was also studied by MacKay
 422 and Aubry [9], who called them rivers. In the work of
 423 MacKay and Aubry continuation ideas were used, while in
 424 the present work a large-scale mechanism which stabilizes
 425 these structures is determined. This stabilization process is
 426 due to the trapping by their self-consistent Peierls-Nabarro
 427 potential.

428 **V. POLYGONS AND OTHER SHAPES**

429 Building on the thin rectangular vortex, we can construct
 430 vortices of arbitrary shape by adding straight line segments,
 431 parallel to the coordinate axes, to make a polygonal path.
 432 Clearly the phase will have to increase by 2π after a circuit
 433 of this polygonal vortex. Therefore, if the vortex has a total
 434 length D , it will be assumed that the phase increases at the
 435 uniform rate $\dot{\theta} = 2\pi/D$ along the polygonal vortex. The same
 436 arguments used for the straight line vortices can be applied to

each side of the vortex, each side acting as an independent 437
 structure. Again instability is observed for δ sufficiently 438
 large. As for the straight line vortex the instability initiates at 439
 the corners, which are the ends of the straight line segments. 440
 An example of such a segmented, stable vortex, which has 441
 an L shape, is shown in Fig. 4. This L shape was obtained 442
 from the evolution of an initial condition constructed with 443
 straight line vortices, with a phase which increases at a rate 444
 $\dot{\theta} = 2\pi/D$, where D is the total length of the vortex. 445

Finally this same construction of complicated vortices 446
 from fundamental units can be used to construct the figure of 447
 8 vortex shown in Fig. 5. This shape was obtained by evol- 448
 ving two circular vortices, as in Fig. 1, after deleting the inner 449
 portions. The phase again has a constant rate of increase 450
 around the vortex, for a total change of 2π . 451

It is clear that this construction of vortices or rivers with 452
 complicated shapes can be continued. Again these vortices 453
 will be stable for very discrete lattices, that is for $\delta \ll 1$, and 454
 as δ increases they will be become destabilized and so decay. 455

In addition to time periodic solutions, the two- 456
 dimensional DNLS equation appears to support a class of 457
 more general localized solutions that are an approximate su- 458
 perposition of breathers with different frequencies. For these 459
 solutions we have a set of active sites U , where for m, n for 460
 these active sites U we have $u_{mn} \sim C_{mn} e^{i\omega_{mn} t}$ with C_n 461
 $\sim 1 \pm \delta$, otherwise $u_{mn} \sim O(\delta)$. The amplitudes C_{mn} and fre- 462
 quencies ω_{mn} for the active sites appear to vary slowly in 463
 time to within a small percentage of some average value that 464

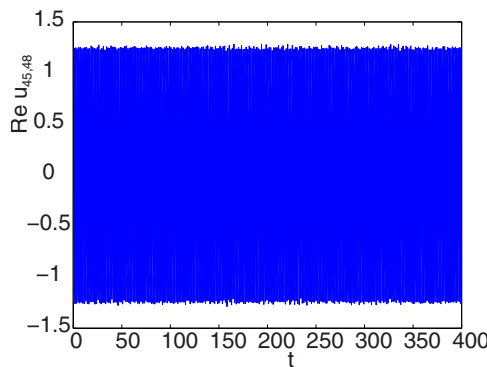


FIG. 8. (Color online) $\text{Re}(u_{48,48})$ at sites of inner square as a function of time.

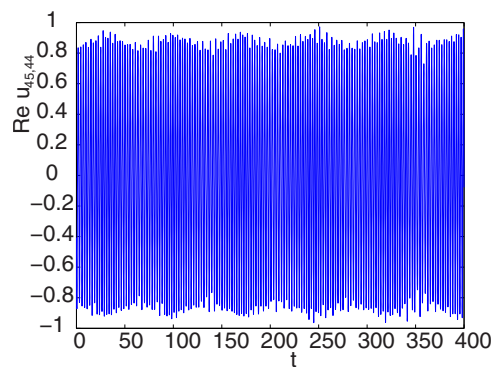


FIG. 10. (Color online) $\text{Re}(u_{45,44})$ at sites of outer square as a function of time.

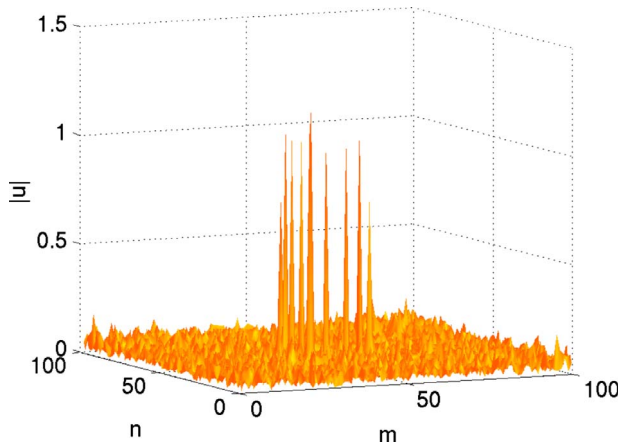


FIG. 11. (Color online) L-shaped solution of the DNLS equation, $\delta=0.2$.

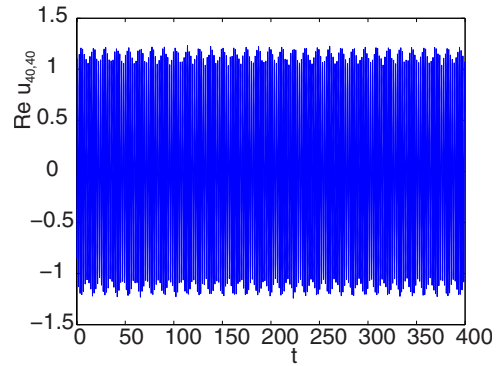


FIG. 13. (Color online) $\text{Re}(u_{40,40})$ as a function of time.

465 depends on the site. Unlike the case for breather (vortex)
466 solutions, we observe that the ω_{mn} are not the same for all
467 active sites.

468 An example can be seen in Fig. 6, where we have used
469 periodic boundary conditions with $\delta=0.2$ and $\gamma=1.0$. The
470 peaks are seen clearly in the contour plot shown in Fig. 7.
471 They are located at the three sets of sites

472
$$U_1 = \{(48, 48), (53, 48), (53, 53), (48, 53)\},$$

473
$$U_2 = \{(47, 46), (54, 46), (54, 54), (47, 55)\},$$

474
$$U_3 = \{(45, 44), (56, 44), (56, 57), (44, 57)\},$$

475 of a 100×100 lattice. Each U_j defines a parallelogram, with
476 U_1 the “inner,” U_2 the “middle,” and U_3 the “outer” paral-
477 lelogram. In Figs. 8–10 we show the real parts of u at the
478 sites $(48, 48) \in U_1$, $(47, 46) \in U_2$, and $(45, 44) \in U_3$. The val-
479 ues of u at all four sites in each U_j are seen to be identical to
480 the corresponding three representative sites shown in the fig-
481 ures. We furthermore see that the (average) amplitudes for
482 U_1 , U_2 , and U_3 are 1.25, 0.92, and 0.83, respectively. The
483 corresponding (average) periods for U_1 , U_2 , and U_3 are 1.60,
484 2.24, and 2.70. Comparing the amplitudes of the three U_j , we
485 see some periodic energy interchange between the middle

and outer parallelograms. The different average frequencies 486
in each parallelogram imply that these solutions are not 487
breathers, but rather an approximate superposition of three 488
slightly modulated breather solutions. Similar solutions are 489
seen for periodic and free boundary conditions on the finite 490
lattice. In both cases the localized solutions appear to be 491
stable in that we do not see any tendency for the amplitudes 492
of the main peaks to diminish. Adding a small boundary 493
damping with $\nu \leq 10^{-2}$ as in [5] does not alter the amplitudes 494
of the peaks over several hundreds of periods. 495

A second example is seen in Fig. 11, with the correspond- 496
ing contour plot shown in Fig. 12. The L-shaped pattern of 497
peaks consists of the corner sites $(40,40)$ and $(41,41)$ and the 498
four pairs of sites $U_1 = \{(40,45), (45,40)\}$, U_2 499
 $= \{(40,51), (51,40)\}$, $U_3 = \{(40,55), (55,40)\}$, and U_4 500
 $= \{(40,58), (58,40)\}$. The motion of the two sites in each U_j 501
is identical. In each site we see an oscillation with a slow 502
modulation; see, e.g., Figs. 13 and 14 where we show the 503
real part of u_{mn} at the sites $(m,n) = (40,40)$ and $(58,40)$, re- 504
spectively. The average frequencies at the different U_j are 505
different, for example at $(40,45)$, $(40,55)$, and $(40,55)$ we see 506
the frequencies 1.80, 1.90, and 2.85, respectively. The 507
L-shaped pattern is therefore not a breather, but rather an 508
approximate superposition of six breathers peaked at $(40,40)$, 509
 $(41,41)$, and the four U_j . There is also evidence of some 510
energy interchange between the peaks at $(40,40)$ and $(41,41)$. 511
As for the first example, similar solutions are observed for 512
both periodic and free boundary conditions and the peaks 513
persist under small boundary damping. 514

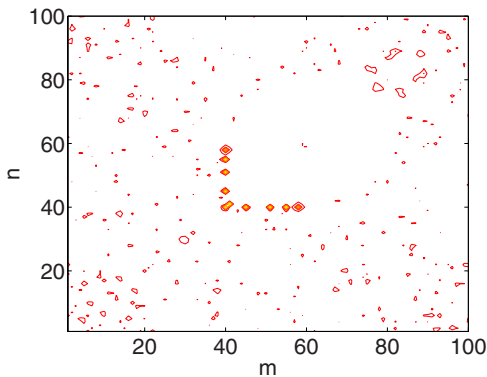


FIG. 12. (Color online) Contour plot of L-shaped solution of the DNLS equation.

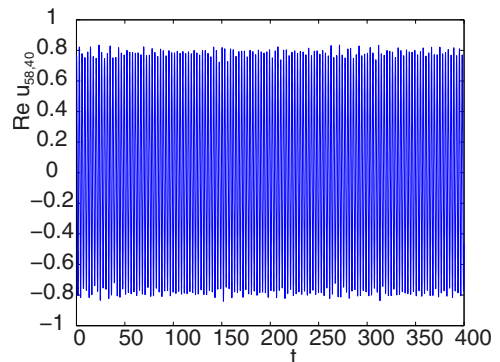


FIG. 14. (Color online) $\text{Re}(u_{58,40})$ as a function of time.

515 VI. CONCLUSIONS

516 It has been shown that discrete lattices can sustain stable,
517 periodic vortices of arbitrary shape with a linearly increasing
518 phase. A modulation theory was developed which explained
519 the stability of these vortices. In particular this modulation
520 theory included the Peierls-Nabarro potential generated by
521 the continuum vortices and was found to be responsible for
522 the stability for δ sufficiently small. The approximate solu-
523 tions of this modulation theory show how the discreteness of
524 the lattice stops the breakup of the vortices. This mechanism
525 is very different from that which stabilizes vortices in nem-
526 atic liquid crystals, as in this continuous medium nonlocality
527 decreases the destabilization terms [18]. For the present dis-
528 crete media the Peierls-Nabarro potential stabilizes the dis-
529 crete vortices. This Peierls-Nabarro potential is absent in
530 continuous media.
531 For the case of straight line vortices it was found that the
532 finite size of the vortex produces waves which travel from its
533 edges toward its center, producing a modulated mean level
534 whose length scale is the length scale of the vortex. This
535 mean level change produces the Peierls-Nabarro potential
536 which traps the vortex.
537 In general, the vortices are sustained by the Peierls-
538 Nabarro potential, which traps them at a minimum, with the
539 same potential preventing their breakup. On the other hand,
540 as the lattice approaches the continuum limit, the potential is
541 no longer sufficient to trap them, so that they collapse.

568
569
570

571 [1] D. N. Christodoulides and R. I. Joseph, *Opt. Lett.* **13**, 794
572 (1988).
573 [2] A. B. Aceves, C. de Angelis, T. Peschel, R. Muschall, F. Leder-
574 erer, S. Trillo, and S. Wabnitz, *Phys. Rev. E* **53**, 1172 (1996).
575 [3] R. Morandotti, U. Peschel, J. S. Aitchison, H. S. Eisenberg,
576 and Y. Silberberg, *Phys. Rev. Lett.* **83**, 2726 (1999).
577 [4] D. N. Christodoulides, F. Lederer, and Y. Silberberg, *Nature*
578 (London) **424** 817 (2003).
579 [5] R. Livi, R. Franzosi, and G. L. Oppo, *Phys. Rev. Lett.* **97**,
580 060401 (2006).
581 [6] G. Kopidakis, S. Aubry, and G. P. Tsironis, *Phys. Rev. Lett.*
582 **87**, 165501 (2001).
583 [7] S. Aubry, *Physica D* **216**, 1 (2006).
584 [8] A. J. Sievers and S. Takeno, *Phys. Rev. Lett.* **61**, 970 (1988).
585 [9] R. S. MacKay and S. Aubry, *Nonlinearity* **7**, 1623 (1994).
586 [10] M. I. Weinstein, *Nonlinearity* **12**, 673 (1999).
587 [11] J. M. Bergamin, T. Bountis, and C. Jung, *J. Phys. A* **33**, 8059

It should be remarked that the present modulation theory **542**
 approach gives accurate predictions in simple terms for both **543**
 the qualitative and quantitative features of the evolution. **544**

A further feature of some of the localized solutions exam- **545**
 ined here is a temporal behavior that is unlike that of the **546**
 well-known breather solutions. Such localized solutions may **547**
 correspond to exact solutions of the infinite lattice, or to **548**
 slowly decaying states that may be close to exact solutions **549**
 for finite lattices. Possible subtle differences between the **550**
 stable localized states in finite and infinite lattices can be due **551**
 to slow decay due to radiation in the infinite case [16]. These **552**
 differences may be difficult to capture numerically, but may **553**
 give distinct long-time predictions for optical vs molecular **554**
 or condensed matter systems modeled more realistically by **555**
 the DNLS equation on finite and infinite lattices, respec- **556**
 tively. **557**

Similar ideas to those developed here could be used for **558**
 the study of other types of vortices, such as nonlocal discrete **559**
 vortices. This is the subject of ongoing studies. **560**

ACKNOWLEDGMENTS **561**

The authors would like to thank Professor Yuri Kivshar **562**
 for discussions about and insights into the work presented in **563**
 this paper. This research was supported by the Engineering **564**
 and Physical Sciences Research Council (EPSRC) under **565**
 Grant No. EP/D075947/1 and by CONACyT under Grant **566**
 No. 50303. **567**

(2000). **588**
 [12] D. E. Pelinovsky, P. G. Kevrekidis, and D. J. Frantzeskakis, *Physica D* **212**, 20 (2005). **589**
 [13] M. J. Ablowitz and Z. H. Musslimani, *Phys. Rev. Lett.* **87**, **591**
 254102 (2001). **592**
 [14] A. Fratolocchi and G. Assanto, *Phys. Rev. E* **72**, 066608 **593**
 (2005). **594**
 [15] R. Carretero-González, J. D. Talley, C. Chong, and B. A. Mal- **595**
 omed, *Physica D* **216**, 77 (2006). **596**
 [16] D. Bambusi and D. Vella, *Discrete Contin. Dyn. Syst., Ser. B* **597**
2, 389 (2002). **598**
 [17] G. B. Whitham, *Linear and Nonlinear Waves* (John Wiley and **599**
 Sons, New York 1978). **600**
 [18] A. A. Minzoni, N. F. Smyth, A. L. Worthy, and Y. S. Kivshar, *Phys. Rev. A* **76**, 063803 (2007). **601**
 [19] L. A. Cisneros and A. A. Minzoni, *Physica D* (to be **602**
 published). **603**
604

AUTHOR QUERIES —

#1 please check extent of sech function

#2 please check